Sensitivity of resonance properties of all-dielectric multilayers driven by statistical fluctuations

Aude L. L. Lereu, F. Lemarchand, M. Zerrad, D. Niu, V. Aubry, A. Passian, C. Amra

Research Article | Vol. 27, No. 21 / 14 October 2019 / Optics Express 30654

Optics EXPRESS

Sensitivity of resonance properties of all-dielectric multilayers driven by statistical fluctuations

A. L. Lereu,[1,*] F. Lemarchand,[1] M. Zerrad,[1] D. Niu,[1,2] V. Aubry,[2] A. Passian,[3] and C. Amra[1]

[1]Aix Marseille Univ, CNRS, Centrale Marseille, Institut Fresnel, Marseille, France
[2]PSA Groupe, Direction Scientifique, Centre Technique de Vélizy, Vélizy-Villacoublay, F-78140, France
[3]Quantum information Science, Oak Ridge National Laboratory, Oak Ridge, TN 37830, USA
[*]aude.lereu@fresnel.fr

Abstract: In photonics and emerging fields of quantum and topological materials, increasing demands are placed upon the state and control of electromagnetic fields. Dielectric multilayer materials may be designed and optimized to possess extremely sharp spectral and angular photonic resonances allowing for the creation of fields orders of magnitude larger than the exciting field. With enhancements of 10^4 and higher, the extreme nature of these resonances places high constraints on the statistical properties of the physical and optical characteristics of the materials. To what extent the spectral and angular shifts occur as a result of fluctuations in the refractive indices and morphologies of the involved low-loss subdomains have not been considered previously. Here, we present how parameter variations such as those caused by fluctuations in deposition rate, yielding bias, random and compensated errors, may affect the resonance properties of low-loss all-dielectric stacks.

1. Introduction

Numerous work have been reported on dielectric multilayers optimization using both Bloch surface waves [1–13] or admittance formalism in the total internal reflection conditions [14–19] towards giant field enhancement generation [20–27]. Because of the geometric similarities, the optical response of the optimized dielectric multilayers (DM) is often compared [28–31] with plasmon excitation [32–36] in metal thin films [37]. Resonant DMs can achieve giant optical fields when tuned to their sharp spectral or angular resonances. Similar to plasmonic systems, DMs applications are numerous encompassing sensing [29,38–45], diagnostics [46,47], and/or imaging [48–54]. These applications leverage the DMs' enabling of higher sensitivity, better limit of detection, increase in fluorescence emission intensity, and emission lifetime decrease. Unlike plasmonic systems, DMs exhibit low losses, are not severely limited with respect to the specific subdomain material types, and can be highly optimized for excitation beams with any incident angles and wavelengths. Major advances were presented by Amra et al by introducing the concept of zero-admittance layer (ZAL) [55]. ZALs, allowing for the generation of multiple resonances at different incident angles or excitation wavelengths, achieves field enhancement with arbitrary localization within the stack, i.e., not limited only to the free interface, and irrespective of the effect of the substrate. The configurational flexibility of ZALs can open new opportunities in the field of microcavities or low threshold laser sources. Note that, in the homogenization limit, we expect the fluctuations in the film properties may stimulate similar effect as in the case of effective medium approximation for various particle inclusion scenarios as reported in [56] using particle swarm optimization applied to Bruggeman homogenization formalism.

The superior resonance properties of the DMs, a great asset in sensing and imaging applications, place stringent requirements on the interacting field with respect to the spectral and angular

#367693 https://doi.org/10.1364/OE.27.030654
Journal © 2019 Received 15 May 2019; revised 26 Jul 2019; accepted 28 Jul 2019; published 9 Oct 2019

Optics EXPRESS

bandwidths, which could be affected by fluctuations propagated in the optical thicknesses, e.g., via fabrication errors or environmental parameters. If unresolved, such fluctuations can deteriorate the resonance quality limiting the full potential of the DMs. By evaluating the bandwidths of the optical illumination for different DMs, one may conclude that the angular divergence is a limiting factor with respect to the excitation wavelength. This can be seen from Fig. 1, which summarizes our previous results [57] using three DMs designed for a field enhancement factor of $\mathcal{F} = |E|^2/|E_0|^2 = 10^5, 10^4, 10^3$, where E_0 and E are the incident and the corresponding resulting field at the free interface, respectively. From these results one may conclude that for $\mathcal{F}>10^4$, we have to control the divergence to a precision that is currently not realizable. Therefore, we will focus on optimization and fabrication of DMs for $\mathcal{F}=10^4$, the highest realizable $\mathcal{F}$. We investigate here fabrication errors and their effects on the resonance characteristics of the DM by introducing either bias, or random, or compensated errors in the DM design. Indeed, the realization of a multilayer is necessarily tainted with fabrication errors which are related to the deposition technology, to the thickness control technique (optical, quartz, stopwatch ...) and the multilayer design itself [58].

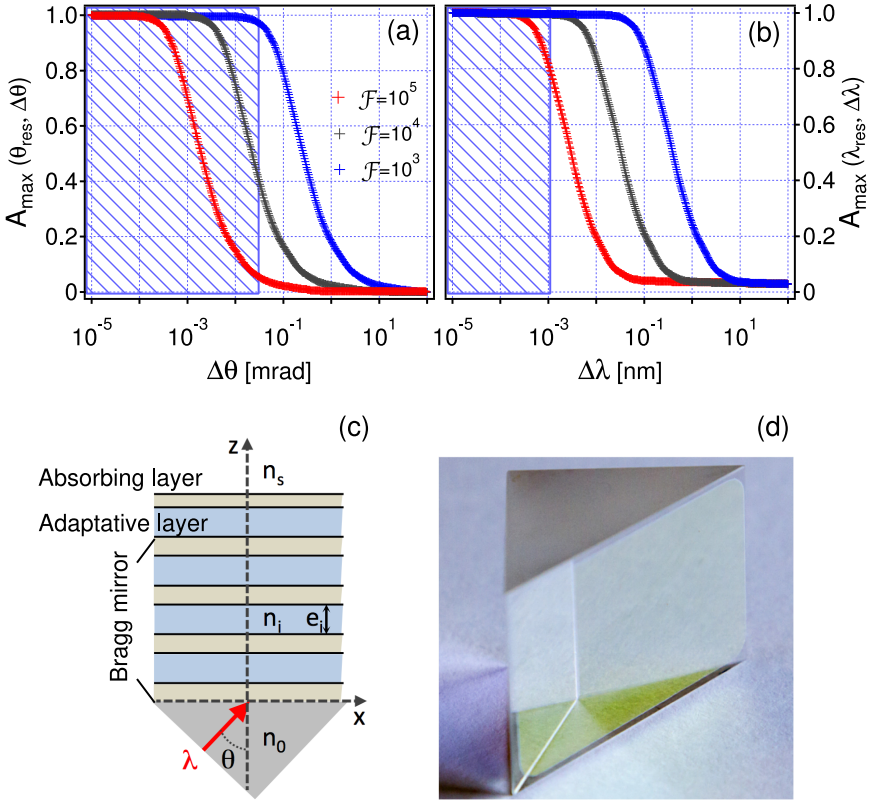

Fig. 1. Maximum of absorption as a function of angular divergence $\Delta\theta$ (a) and spectral bandwidth $\Delta\lambda$ (b). Dielectric multilayers have been optimized for sustaining field enhancement factor $\mathcal{F}$ of 10^5 (red), 10^4 (grey) and 10^3 (blue). The hatched regions mark the experimental regions currently not achievable, for more details refer to [57]. (c) Scheme of a resonant dielectric multilayer under total internal reflection illumination with the absorbing and adaptative layers and the Bragg mirror. (d) Example of realization of a resonant DM on a prism.

Optics EXPRESS

The basic principle for optical control of thin solid film deposition [59] is that for a thin layer illuminated at a given controlled wavelength λ_c, extremum in the transmission is achieved whenever the optical thickness ne is a multiple of a quarter of this wavelength with $n(\lambda_c)e = p\lambda_c/4$, p being the number of extremum occurrences. This result remains true if the thickness increases on a multilayer already manufactured, provided that it is of real admittance. So, with taking into account the spectral dispersion of the refractive indices, the deposition thickness e can be controlled, using a monochromator by observing the number p of extremum occurrences via $e = p\lambda_c/4n(\lambda_c)$. To make the DMs, we used a white light source going through the superstrat on which the deposition is ongoing where we select the proper controlled wavelength in real time and we observe the transmission T (t, λ_c) over the deposition time. Provided that the deposition rate $v = de/dt$ is quasi-constant, the resulting extrema are then identical to those of T(e, λ_c). To spot these extrema, we carry out a real time derivation of the control signal and we stop the deposit as soon as the derivative goes through a zero [59].

We then see a first source of errors comes from the quantity of matter that continues to be deposited from the moment when the stop command was launched and when the "evaporating" is occulted. We are thus witnessing a first type of systematic error similar to a "bias". Moreover the identification of the zeros of the derivative is naturally tainted with errors on either side of these zeros, hence the appearance a second type of "random" error. These latter errors may be partially "compensated" in the case of a monochromatic control for all the stacking and for conditions of use in normal incidence. The component is then much more robust, which justifies the generalization of monochromatic optical control to all complex optical filters with narrow band (as presented here). On the contrary for the fabrication of broadband filters, a "Broadband" control is particularly well suited [60,61].

We consider here the bias errors associated with systematic differences between the theoretical and measured values of the refractive indices n and the physical thicknesses e. We will then apply random and compensated errors on the deposited thickness to evaluate independent errors on a specific or each layer(s) of the DM.

2. Results and discussion

Beforehand, we recall that in optical thin film coatings optimization [62], one can introduce the complex admittance Y defined as the ratio of the magnetic field H over the electric field E when working under plane waves illumination and with linear, isotropic and homogeneous media. We have developed two related optimization methods using the admittance law: 1- consisting in maximizing the absorption A and minimizing the reflection R so, as we are under total internal reflection (i.e. the transmission T=0 is purely evanescent), $A = 1$ and $R = 0$, see [17,27] for calculation details, in this case, starting from the substrate, a bilayer is added to leave the imaginary axis and reach the real axis of the admittance, then a quaterwave multidielectric mirror matched for oblique incidence with $k_{Sub}<\sigma<k_L<k_H$, with σ the spatial pulsation and k_i the wavevectors of each materials/media, so that the field in the substrate is evanescent but trigonometric in the stack ; 2- consisting in adding a unique non-absorbing zero-admittance layer (ZAL) over a matched quaterwave multidielectric mirror similar to the first strategy, by controlling the thickness of this unique layer, see [55] for calculation details. Using a ZAL allows in one step to leave the Y imaginary axis and reach the real one. As illustrated in Fig. 1(c), the resulting multidielectric layers are an alternance of high and low refractive indices materials deposited on a prism to experimentally achieve total internal reflection. The presented fabricated DM was optimized here for a TE-polarized excitation beam of wavelength λ_{res}=633 nm and an incident angle of θ_{res}=45° as depicted in Fig. 1(c). An example of realization is given in Fig. 1(d).

Optics EXPRESS

2.1. Bias errors

We begin our discussion by considering variations on the optical index n and/or in the layer thickness e that can occur, for example, when the control detector of the deposition system or any measurements of n and e exhibit a bias. Thus, differences between the theoretical values and those corresponding to the actual measured n or deposited e, are assumed to be the same for every layers. Application of 0.1- 3% relative errors δn over n or δe over e, linked to the bias, as $b_x x = x \pm \delta x$ with $x = n$ or e, to each layer covers a realistic thin film deposition operation. The considered error range is sufficient for the resulting structure to differ from the original optimized stack, as discussed below.

When the stack behaves as a quarter-wave element at the new incident angle and associated excitation wavelength, the shifted resonance positions can be predicted. Indeed, during optimization, each layer optical thickness is expressed as:

$$n_i(\lambda_{res})e_i\cos\theta_i = \lambda_{res}/4, \tag{1}$$

with λ_{res}, the resonance wavelength, $n_i(\lambda_{res})$, e_i and θ_i the refractive index, the thickness and the incident angle of the i^{th} layer, respectively. With the bias b_e applied to the thicknesses, Eq. 1 is modified as:

$$\begin{aligned} n_i(\lambda_{res})(e_i + b_e)\cos\theta_i &= \lambda_1/4, \\ \text{if} \quad n_i(\lambda_{res})b_e\cos\theta_i &= (\lambda_1 - \lambda_{res})/4, \end{aligned} \tag{2}$$

with λ_1 being the new resonance wavelength. Thus, the new resonance positions can be easily calculated for low values of biases. Note that this can be transposed to applied optical index biases.

We consider biases b_n applied to the refractive indices or b_e applied over the deposited thicknesses and we study the effect as a function of incident angles, keeping the incident wavelength fixed. Denoting the refractive index at the free interface with n_S, from the specific spatial frequency σ_{res} at which the DM was optimized:

$$\sigma_{res} = 2\pi n_S \sin(\theta_{res})/\lambda_{res}, \tag{3}$$

it can be seen that the new biased structures with measured indices $n_i \pm \delta n$ or deposited thicknesses $e_i \pm \delta e$, can be resonant when tuning either the incident angle and/or the excitation wavelength.

The tunability can be further studied from the dispersion relation of the stack as a function of the thickness of the last layer e_N and incident angle (Fig. 2(a)) and as a function of wavelength and incident angle (Fig. 2(b)). The reflectance was here computed for $e_N \pm 5$ nm, and $\lambda \pm 30$ nm and the angular range from $+5°$ to $-2.2°$ (to stay under total internal reflection condition).

The responses of the DM in absorption, angular shift and field enhancement are thus given in Fig. 3 and Fig. 4. Applying an identical bias to every layer, it can be shown that the overall behavior of the absorption curve is globally preserved. Figure 3(a) shows that the absorption peaks are shifted towards higher (lower) resonant angles for positive (negative) error values of n. Similar observations are done for variations over e (data not shown). The maximum of absorption decreases by less than 1% over n, see Fig. 3(d), and by ≈3% over e see Fig. 4(a). The applied biases affect mainly the absorption by shifting the illumination conditions. This shift in incident angle, given in Fig. 3(d) and Fig. 4(b), varies from θ_{res} to θ_1, where θ_1 is function of the biased stack (see Eq. 2) and can be extracted by locating the maximum of absorption (Fig. 3(a)), noting $\theta_1 = \theta_{res}$ when no bias.

Biases also impact the field distribution, and are calculated with respect to the illumination conditions: first, at the frequency σ_{res} from the optimized stack (Fig. 3(b)), second, at the biased conditions, i.e., θ_1 and λ_{res} (Fig. 3(c)). Biases as small as 0.1% have immediate consequences on the field distribution.

Optics EXPRESS

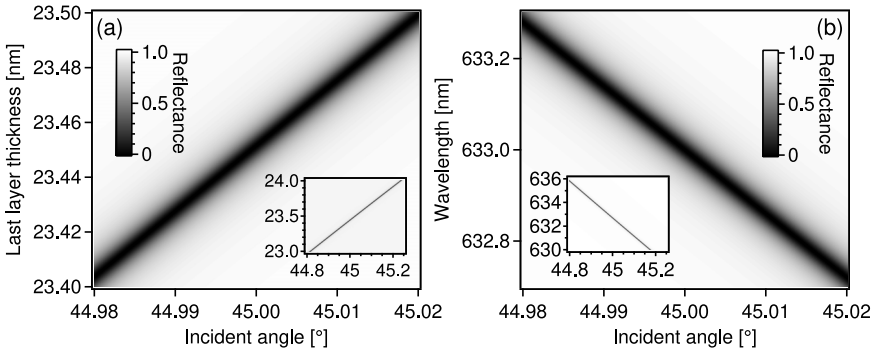

Fig. 2. Dispersion relation mappings as a function of the last layer thickness e_N (± 0.5nm) and the incident angle (± 0.2°) in (a) and as a function of the wavelength (± 3nm) and the incident angle in (b). The reflectance varies linearly in the considered ranges of thicknesses, angles and wavelengths. This shows the tunability of the resonant dielectric multilayer and that one can either tune the incident angle or the excitation wavelength.

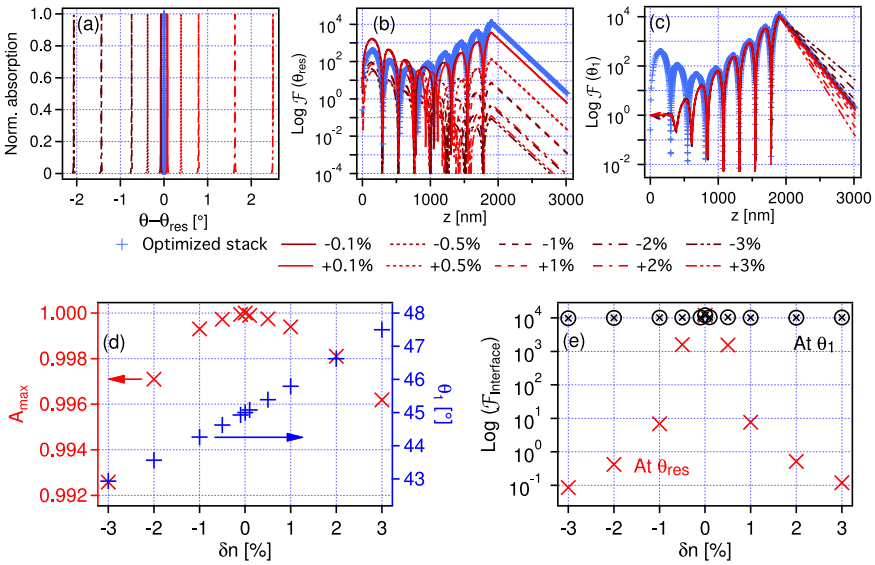

Fig. 3. Effect of a bias on the refractive indices n applied on every layers constituting the resonant DM. Numerical estimations of absorption (a) and field distribution through the stack at the frequencies σ_{res}=(λ_{res}, θ_{res}) (b) and σ_1=(λ_{res}, θ_1) (c). The maximum of absorption (red cross in (d)) and the associated θ_1 (blue cross in (d)) are extracted for each biased structure. The field enhancements at the free interface for both σ_{res} (red cross) and σ_1 (black symbol) are given in (e) as a function of indices error δn induced by a bias b_n applied to every layers.

Under σ_{res}, the field distribution is modified as we increase the fabrication errors; the field enhancement factor decreases by 3 decades for δn=1% (Fig. 3(e)) and by 2 decades for δe=2% (Fig. 4(c)). This shows the importance of determining the refractive index of each material in thin film form prior to deposition. Furthermore, as the bias increases, that is, as we derive from the original optimized DM, the angular variations of the resonance peak increase together with a large degradation of the field enhancement. Under the second illumination conditions, i.e. the new resonance condition, the field enhancement at the free interface is nearly fully conserved

Optics EXPRESS

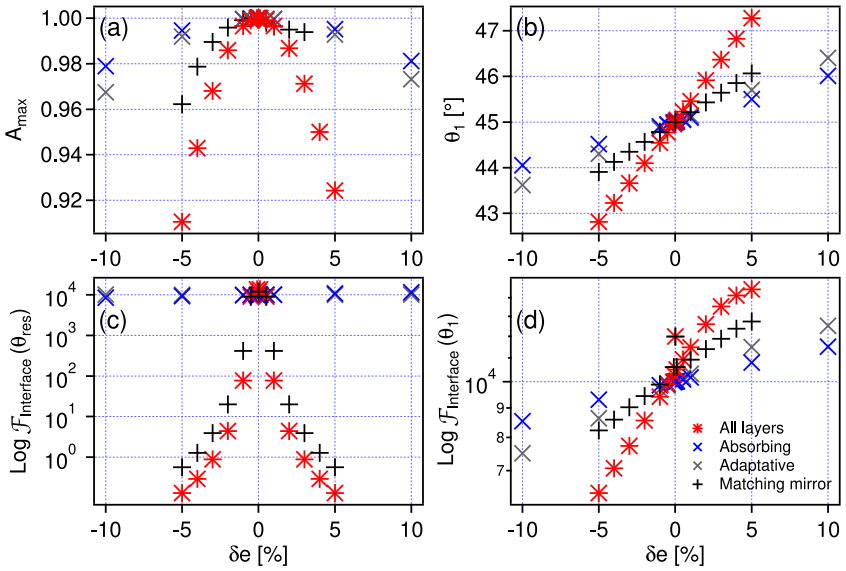

Fig. 4. Effect of biases b_e inducing thickness error δe on the deposited thicknesses e over the maximum of absorption (a) and the associated angle θ_1 (b), and the field enhancement at the free interface for both σ_{res} (c) and σ_1 (d). The red symbols are for δe applied on every layers of the stack, the blue cross for δe on the last absorbing layer, the grey cross for δe on the adaptative layer and the black cross on all the layers constituting the matching mirror.

(black symbols in Fig. 3(e) and red symbols in Fig. 4(d)). However, as predicted, when modifying the incident angles to compensate the bias errors, the penetration depth at the free interface either decreases as θ_1 increases (i.e., higher n or e) or increases as θ_1 decreases (i.e., lower n or e) as evidenced in Fig. 3(c). Finally, note that in Fig. 4, we have also separately evaluated the impact of bias error on the individual last two layers (blue and grey symbols) and only on the Bragg mirror part (black symbols) of the structure (see Fig. 1(c)). We evidenced here that if the last layer thickness may be a critical parameter in term of optimization, the mismatch of the Bragg mirror has even a stronger effect over the fabrication errors.

In conclusion, the applied biases over measurements of n and deposition of e drastically affects the DM's optical response in terms of absorption and field enhancement as the resonance conditions are shifted. Nevertheless, this systematic error can be reduced or even canceled when adapting the spatial frequency from σ_{res} to σ_1. In doing so, the last parameter to be compromised is the penetration depth of the field in the free space.

2.2. *Random errors*

Random errors stemming from time dependent variations in the measurements or deposition, for example, due to temperature or pressure variations during experiment can lead to overvaluation or undervaluation of the measured quantities. Therefore, we consider random fluctuations in the deposited thicknesses e using a set of 50 random structures. By numerically introducing 0.1% - 3% random errors δe on the thickness of every layers i.e. e varies within $[e-\delta e, e+\delta e]$ where δe can take any values in the considered range. As an example, we plot the absorption for the first six random structures as a function of the incident angle for five δe values, as shown in Fig. 5, from where we extract the new incident angle θ_1 for each 50 structures. While observing a shift in the resonance, the maximums of absorption are relatively conserved under proper incident conditions.

Optics EXPRESS

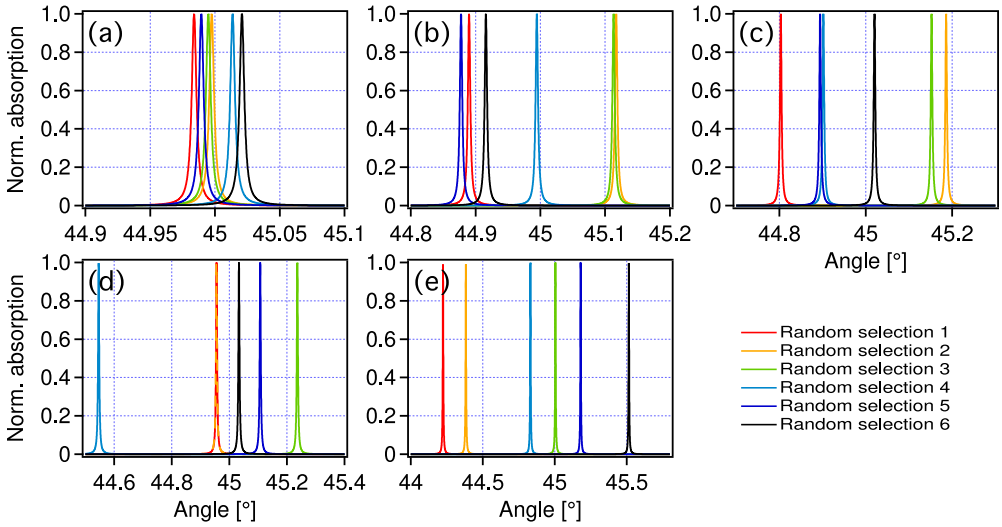

Fig. 5. Numerical absorption of the first six (over 50) random selections of structures when imposing random errors over the thickness of every layers. The applied errors δe are 0.1% in (a), 0.5% in (b), 1% in (c), 2% in (d) and 3% in (e).

Employing the two frequencies σ_{res} and σ_1, further statistical analysis is presented in Fig. 6, where the maximum of absorption, the associated incident angle θ_1 and field enhancement at the free interface are compiled. As can be seen, increasing δe leads to a higher distribution of the maximum of absorption and θ_1. In the extreme case of δe=3%, the probability of obtaining a structure with a 1% reduced absorption (maximum observed drop), is only at 2%. Then θ_1 is distributed over $\theta_{res} \pm 1^\circ$, which is experimentally easily achievable. We note that the resonance conditions can also be compensated by a spectral distribution centered at $\lambda_1 = \lambda_{res} \pm \delta\lambda$. In the presented structure, a variation of $\pm 1^\circ$ is equivalent to a $\delta\lambda$=13nm. Regarding the field enhancement, random errors of 0.1% yields negligible effects. For fixed illumination frequency σ_{res}, the distribution over $\mathcal{F}$ remains around 10^4. But for $\delta e \geq 0.5\%$, the $\mathcal{F}$ at σ_{res} is largely distributed toward lower values of $\mathcal{F}$. For δe=1%, the full range of $\mathcal{F}$ is obtained from 1 up to 10^4, meaning the probability that the 1% random errors can result in a $\mathcal{F}=10^4$ is almost zero. For higher values of δe, $\mathcal{F}$ distribution does not exceed 1500 for δe=2% and 500 for δe=3%. However, when adjusting the incident angle from θ_{res} to θ_1, the $\mathcal{F}$ distributes around $\mathcal{F}_{res}$ of the optimized resonant DM (Fig. 6). The analysis shows that random errors can be fully, or partially (for higher δe), compensated by spectral and/or angular tuning.

The same random error may be applied only to the last layer, that is, the critical layer in our optimization method (Fig. 7). The thickness of the last layer has to be accurately controlled as a δe of 1% (or δe of 5%) on the last layer induces modifications equivalent to a δe of 0.5% (or δe of 2%) over all thicknesses with respect to the absorption and incident angle distribution. However, the field enhancement and distribution within the multilayer remains largely unaffected. This finding is expected despite the criticality of the last layer's thickness in the optimization method. As we tune the excitation parameters to compensate for the fabrication errors, we also introduce a mismatch of the Bragg mirror, implying the need for controlling the thickness of every layers to limit the optical response variations.

Experimentally, the system is subject to both bias and random errors, it behooves us to consider the combined contribution of both types in Fig. 8 for δe_{bias} of $\pm 1\%$ and δe_{rand} of 0.1 and 0.5%. The result of the analysis shows the spreading of the angular position (Fig. 8(a)) as well as the absorption distribution (Fig. 8(b)) with increasing δe_{rand}. Figure 8(c) confirms that angular or

Optics EXPRESS

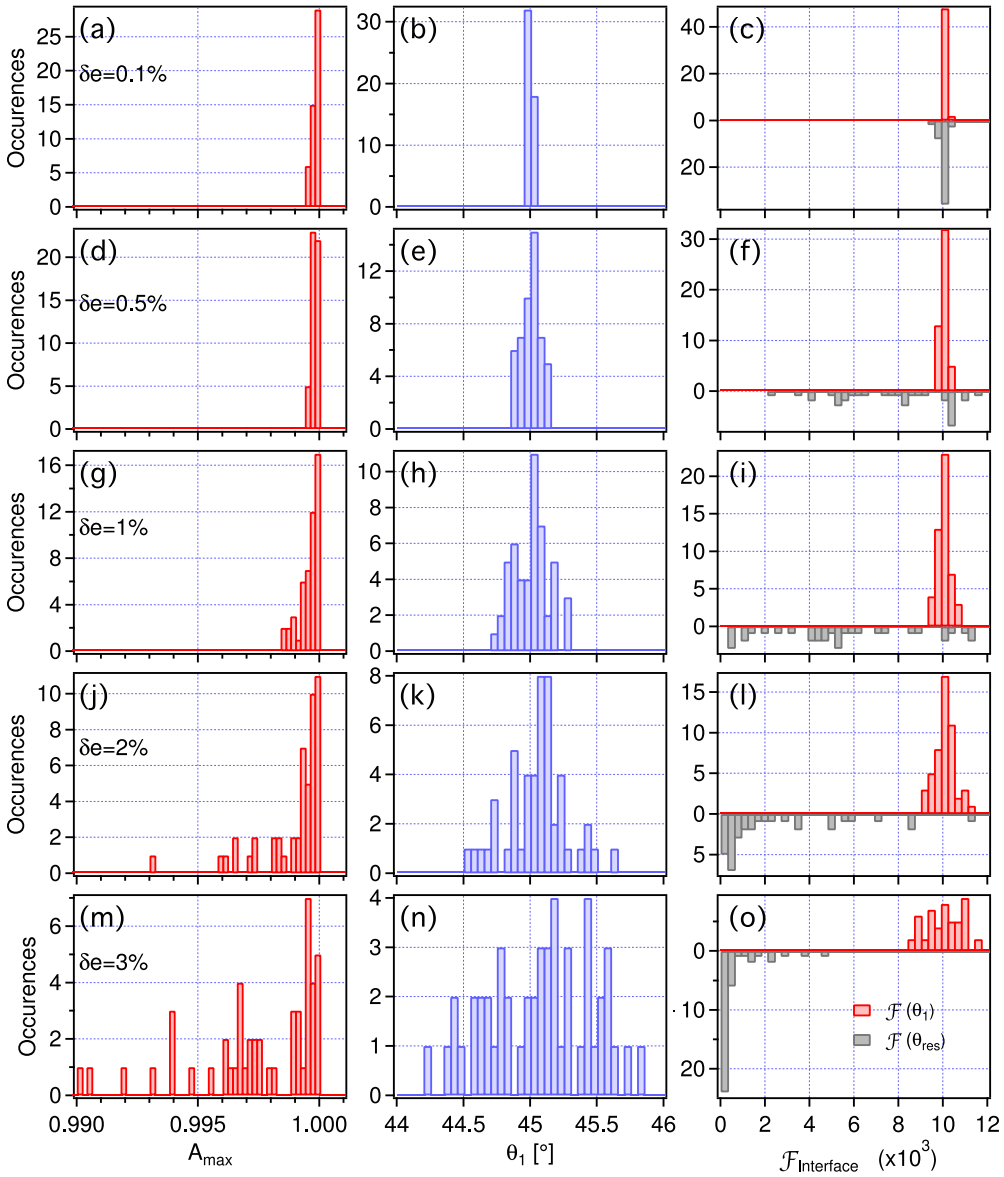

Fig. 6. Histograms over 50 random selections of structures, of the maximum of absorption (first column), the new resonant angle θ_1 (second column) and the field enhancement at the free interface $\mathcal{F}_{Interface}$ (third column) for both spatial frequencies $\sigma_1=(\lambda_{res}, \theta_1)$ (red) and $\sigma_{res}=(\lambda_{res}, \theta_{res})$ (grey). (a-c)δe=0.1%, (d-f) δe=0.5%, (g-i) δe=1%, (j-l) δe=2%, (m-o) δe=3%.

Optics EXPRESS

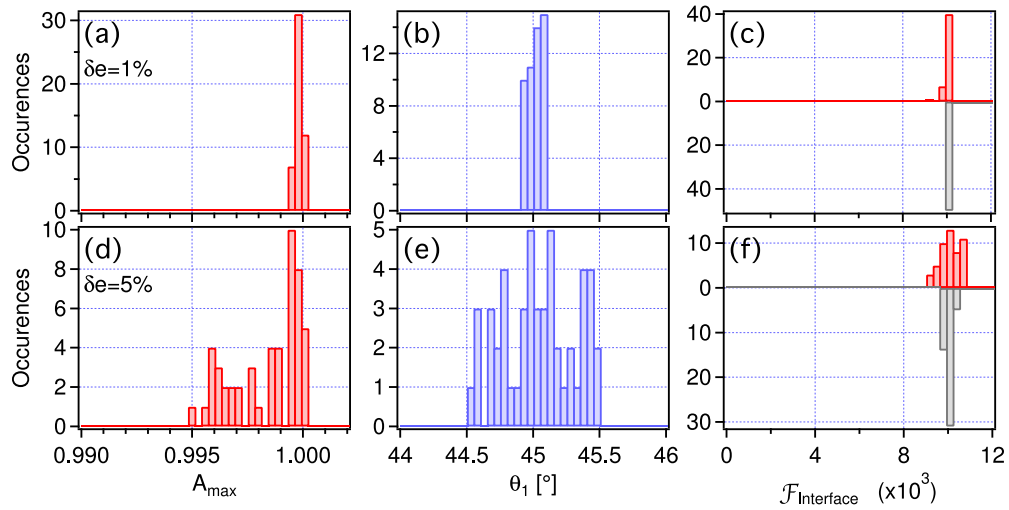

Fig. 7. Histograms over 50 random selections with different last layer thicknesses. The maximum of absorption is given in the first column, the new resonant angle θ_1 in the second column and the field enhancement at the free interface $\mathcal{F}_{Interface}$ in the third column for both spatial frequencies σ_1=(λ_{res}, θ_1) (red) and σ_{res}=(λ_{res}, θ_{res}) (grey). (a-c)δe=1% and (d-f) δe=5%.

spectral tunability allows the field enhancement factor to retain its optimized value. Without compensation on the incident conditions, the field enhancement would decrease by at least two decades, as shown in Fig. 8(d). Finally, as in the case of pure bias error, we observe here that the sign of the bias affects the angular shifts. The values of angle and field enhancement at θ_1 shift toward lower values for negative bias and higher values for positive bias, at least for $\delta e_{rand} < \delta e_{bias}$. Indeed negative bias, yielding smaller thicknesses, directly linked to smaller resonance angles. The latter leads to a faster exponential decay of the field at the free interface (as seen in Fig. 3(c)) and to an increase of the field intensity there.

2.3. Compensated errors

Having estimated the impacts of bias and random errors on the optical response of the resonant DM, we finally investigate the most important errors associated with thin film deposition. Generally, the deposition of a multilayer coating inside a vacuum chamber leads to thickness errors stemming from the in-situ diagnostics and monitoring system. For example, time monitoring of the deposited thickness using a quartz crystal generates random or quasi-random errors following a normal dispersion law. It is well known [63,64] that in-situ optical monitoring, in which a real-time measurement of the incoming flux is made using the coating of a glass slide at a specific controlled wavelength, is more efficient and enables to obtain a more accurate spectral response. Indeed, by analyzing the flux, the optical monitoring adjusts the thickness of the following layer minimizing the influence of the thickness error of the previous coated layer. Through this compensated errors, unlike the case where each layer is considered independently during thin film deposition, we can act on the following layer to compensate errors from the previous layer to get a final component with an optical response as close as possible to the theoretical design. Extending our analysis, we now employ the 15-layers design and consider a single monitoring wavelength of 950 nm, sufficiently different from the design resonance wavelength. The optical monitoring is assumed to occur in normal incidence, where optical signals present a good dynamics [65].

The specific deposition systems employed (equipped with Buhler OMS 5100 optical monitoring system), generate both additive (by 0.002%) and multiplicative (by 0.015%) photometric noise at

Optics EXPRESS

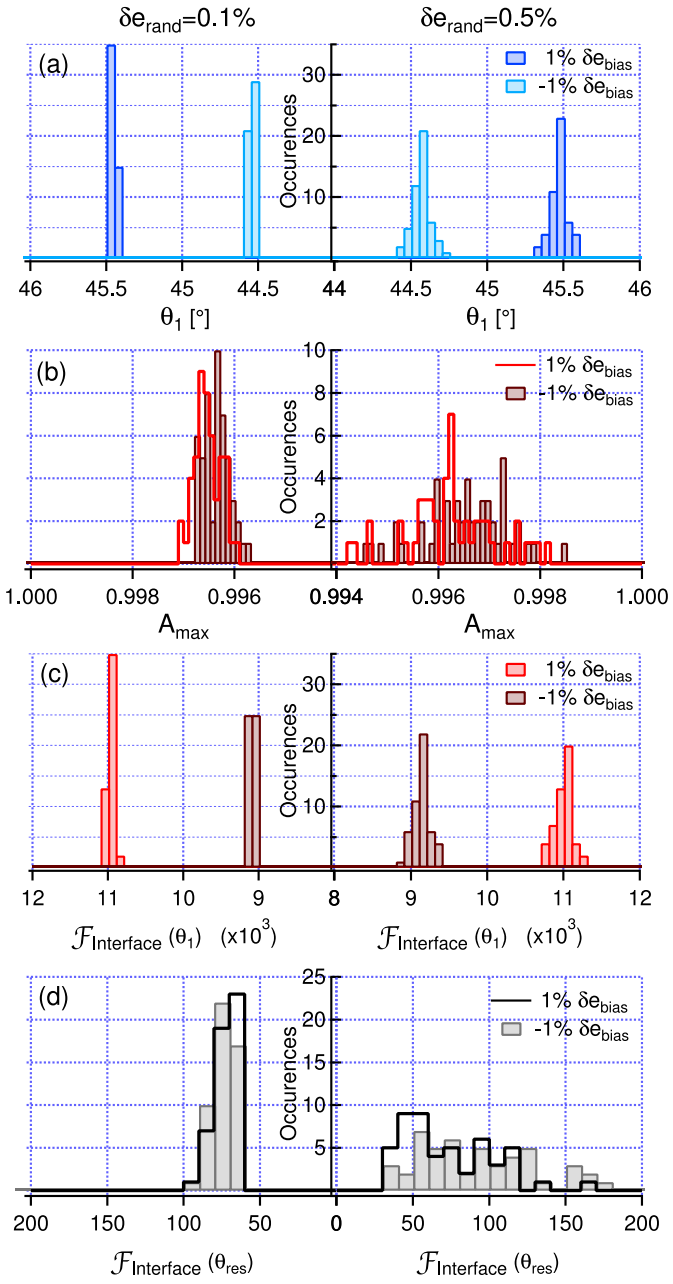

Fig. 8. Histograms over 50 random selections of structures resulting from an imposed bias linked to a δe_{bias} of ±1% with a random error δe_{rand} of 0.1% (first column) and 0.5% (second column).

Optics EXPRESS

a wavelength of 633 nm. By simulating 30 deposition runs, i.e., generating 30 different structures, we calculate the corresponding angular resonance and the field enhancement (Fig. 9(a-c)). Using this deposition technology, the approach yields thicknesses that tend to be under-estimated, which implies that the resulting component will have a resonance slightly below 45°. The optical responses remain relatively conserved with an absorption above 99.9% and a field enhancement above 96% but below 98% with the presented technology with in-situ optical diagnostics and monitoring system. However, to establish an upper limit, we increase the photometric noise by 10, resulting in an additive noise of 0.02% and multiplicative noise of 0.15%.

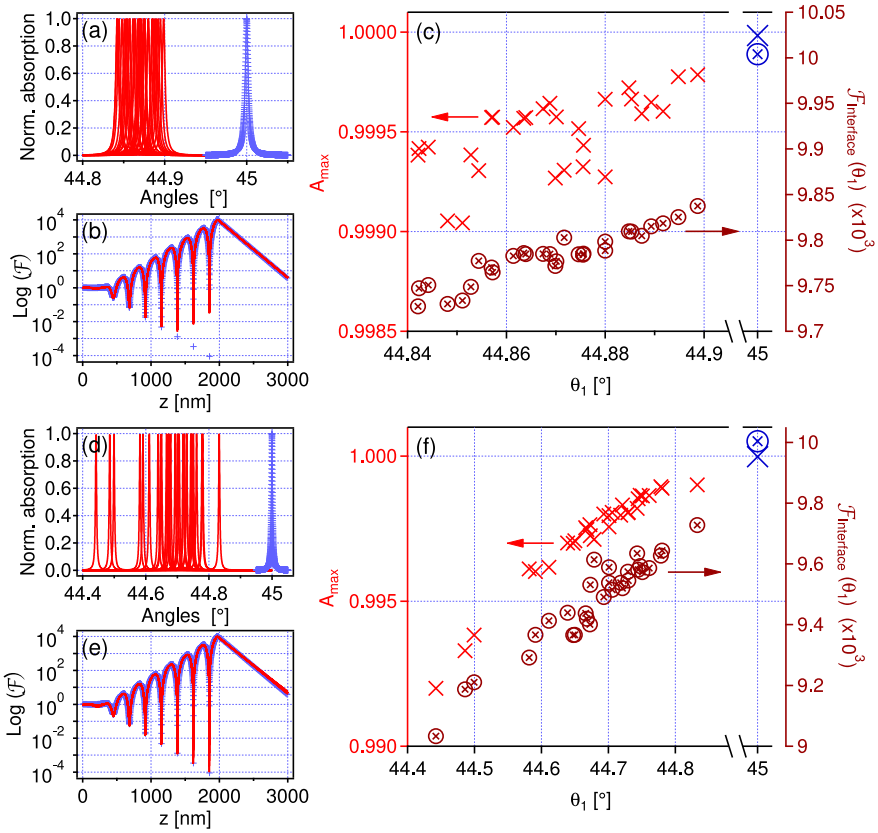

Fig. 9. (a-c) sum up the effect of compensated errors when using an in-situ optical control during deposition. The maximum of absorption stays above 99.9% (red cross in (c)) when adjusting the incident angle between 3.5 to 1.7 mrad (a). The field distribution through the 30 multidielectric stacks in (b) and through the optimized structure (blue symbol in (c)) are very similar with a drop between 96.7% and 97.9% of the field enhancement at the free interface (c). (d-f) illustrate compensated errors with a 10 × noisier in-situ optical control during deposition. The maximum of absorption is kept above 99.2% within an angular range from 10 to 3 mrad. The field distribution in (e) is fairly well conserved with a decrease of the field enhancement at the free interface between 89.5 up to 96.8% with respect to the optimized structure (blue symbol in (e)). Note the blue symbols in each graphs are the values for the optimized structure.

This deposition error corresponds to what may be expected from a typical monitoring system using quartz crystals (Fig. 9(d-f)). Even with such noisy in-situ thickness control, the resulting components are expected to have an optical response very close to that theoretically predicted, given an incident angular adjustment between 0.1 and 0.6°. Reiterating the simulation of 30 runs

Optics EXPRESS

and the calculation of the resonance parameters, we find the resulting absorption to be above 99.2% and the field enhancement to vary between 89% and 97%. This demonstrates that with the actual deposition techniques, the fabrication errors are not disruptive for achieving giant optical field generation in resonant dielectric multilayers. The error compensation contains the effect of fabrication error on the final component optical response and the tunability of the excitation parameters can compensate the remaining effects.

3. Conclusions

The presented study of the illumination bandwidths in [57] facilitates the determination of the effects of fabrication errors impacting the optical thicknesses and thus the optical response of resonant dielectric multilayers. The considered ranges of bias, random, and combined errors in the system parameters of refractive index and physical thicknesses provided a reasonable analysis domain useful for experimental design. From the analysis, we conclude that any errors $\geq 1\%$, in the case of a resonant DM designed for a $\mathcal{F}=10^4$, can drastically affect its optical response. However, we also showed that optical performances are quasi-conserved if the incident conditions (in angles and/or wavelengths) can be sufficiently tuned. The dispersion relation mappings show this relationship with a linearity over large ranges. We considered here a DM with a $\mathcal{F}=10^4$ following the limitations given by the optical bandwidths. However, DMs designed with a $\mathcal{F}=10^3$ is approximately 10 time less sensitive to the bias or random errors (data not shown). For DMs with a $\mathcal{F}$ larger than 10^4, the percentage of error affecting the optical response is expected to be even more critical than the observed 1% here. We stress the need for controlling the thin film deposition, with an accuracy below 1% for each deposited optical thicknesses, in order to minimize the effect on the optical response when both angular and spectral incident conditions are constrained to be fixed by the application. However, when the excitation parameters are not restrictive, the adverse effects can be compensated by a slight tuning of the parameters. Here, the suggested compensation errors took into account the current limitations in optical thin film deposition techniques with optical in-situ controls. The current technology with an in-situ feedback allowing adjustment of the following layer thickness permits fabrication of resonant DMs with errors significantly below than 1%. The optical bandwidths, and specifically the incident beam divergence, remain therefore the main issue for supporting field enhancement up to 10^4 in resonant DM.

Acknowledgments

The authors acknowledge the PSA group for financial support of this work, the ANRT for their support through the CIFRE program and the RCMO Group of the Institut Fresnel for the realization of the coatings. The authors also acknowledge the CNRS and the Aix-Marseille Université. A. P. acknowledges support from the laboratory directed research and development (LDRD) program at the Oak Ridge National Laboratory (ORNL). This work is part of the OpenLab PSA/AMU: Automotive Motion Lab through the StelLab network.

References

1. P. Yeh, A. Yariv, and A. Y. Cho, "Optical surface waves in periodic layered media," Appl. Phys. Lett. **32**(2), 104–105 (1978).
2. W. Ng, P. Yeh, P. C. Chen, and A. Yariv, "Optical surface waves in periodic layered medium grown by liquid phase epitaxy," Appl. Phys. Lett. **32**(6), 370–371 (1978).
3. P. Yeh, A. Yariv, and C-S. Hong, "Electromagnetic propagation in periodic stratified media. I. General theory," J. Opt. Soc. Am. **67**(4), 423–438 (1977).
4. A. Yariv and P. Yeh, "Electromagnetic propagation in periodic stratified media. II. Birefringence, phase matching, and x-ray lasers," J. Opt. Soc. Am. **67**(4), 438–447 (1977).
5. N. Ashby and S. C. Miller, "Interference theory of reflection from multilayered media," J. Opt. Soc. Am. **67**(4), 448–453 (1977).

Optics EXPRESS

6. E. R. Mendieta and P. Halevi, "Electromagnetic surface modes of a dielectric superlattice: the supercell method," J. Opt. Soc. Am. B **14**(2), 370–381 (1997).
7. W. M. Robertson and M. S. May, "Surface electromagnetic wave excitation on one-dimensional photonic band-gap arrays," Appl. Phys. Lett. **74**(13), 1800–1802 (1999).
8. K. Mehrany, S. Khorasani, and B. Rashidian, "Novel optical devices based on surface wave excitation at conducting interfaces," Semicond. Sci. Technol. **18**(6), 582–588 (2003).
9. J. Martorell, D. W. L. Sprung, and G. V. Morozov, "Surface TE waves on 1D photonic crystals," J. Opt. A: Pure Appl. Opt. **8**(8), 630–638 (2006).
10. F. Michelotti, A. Sinibaldi, P. Munzert, N. Danz, and E. Descrovi, "Probing losses of dielectric multilayers by means of Bloch surface waves," Opt. Lett. **38**(5), 616–618 (2013).
11. V. Koju and W. M. Robertson, "Excitation of Bloch-like surface waves in quasi-crystals and aperiodic dielectric multilayers," Opt. Lett. **41**(13), 2915 (2016).
12. R. Wang, H. Xia, D. Zhang, J. Chen, L. Zhu, Y. Wang, E. Yang, T. Zang, X. Wen, G. Zou, P. Wang, H. Ming, R. Badugu, and J. R. Lakowicz, "Bloch surface waves confined in one dimension with a single polymeric nanofibre," Nat. Commun. **8**(1), 14330 (2017).
13. R. Dubey, E. Barakat, M. Hayrinen, M. Roussey, S. K. Honkanen, M Kuittinen, and H. P. Herzig, "Experimental investigation of the propagation properties of bloch surface waves on dielectric multilayer platform," J. Eur. Opt. Soc.-Rapid Publ. **13**(1), 5 (2017).
14. R. C. Nesnidal and T. G. Walker, "Multilayer dielectric structure for enhancement of evanescent waves," Appl. Opt. **35**(13), 2226–2229 (1996).
15. L. Gao, F. Lemarchand, and M. Lequime, "Exploitation of multiple incidences spectrometric measurements for thin film reverse engineering," Opt. Express **20**(14), 15734–15751 (2012).
16. R. Sainidou, J. Renger, T. V. Teperik, M-U. Gonzalez, R. Quidant, and F. J. Garcia de Abajo, "Extraordinary All-Dielectric Light Enhancement over Large Volumes," Nano Lett. **10**(11), 4450–4455 (2010).
17. C. Ndiaye, F. Lemarchand, M. Zerrad, D. Ausserré, and C. Amra, "Optimal design for 100% absorption and maximum field enhancement in thin-film multilayers at resonances under total reflection," Appl. Opt. **50**(9), C382–C387 (2011).
18. C. Amra, C. Ndiaye, M. Zerrad, and F. Lemarchand, "Optimal Design for Field Enhancement in optical coatings," Proc. SPIE **8168**, 816808 (2011).
19. A. L. Lereu, M. Zerrad, C. Ndiaye, F. Lemarchand, and C. Amra, "Scattering losses in multidielectric structures designed for giant optical field enhancement," Appl. Opt. **53**(4), A412–A416 (2014).
20. R. Kaiser, Y. Lévy, N. Vansteenkiste, A. Aspect, W. Seifert, D. Leipold, and J. Mlynek, "Resonant enhancement of evanescent waves with a thin dielectric waveguide," Opt. Commun. **104**(4-6), 234–240 (1994).
21. G. Labeyrie, A. Landragin, J. Von Zanthier, R. Kaiser, N. Vansteenkiste, C. Westbrook, and A. Aspect, "Detailed study of a high-finesse planar waveguide for evanescent wave atomic mirrors," Quantum Semiclassical Opt. **8**(3), 603–627 (1996).
22. P. C. Ke, X. S. Gan, J. Szajman, S. Schilders, and M. Gu, "Optimizing the strength of an evanescent wave generated from a prism coated with a double-layer thin-film stack," Bioimaging **5**(1), 1–8 (1997).
23. M. D. Perry, R. D. Boyd, J. A. Britten, D. Decker, B. W. Shore, C. Shannon, and E. Shults, "High-efficiency multilayer dielectric diffraction gratings," Opt. Lett. **20**(8), 940–942 (1995).
24. J. K. Chua and V. M. Murukeshan, "Resonant amplification of frustrated evanescent waves by single dielectric coating," Opt. Commun. **283**(1), 169–175 (2010).
25. E. Descrovi, T. Sfez, L. Dominici, W. Nakagawa, F. Michelotti, F. Giorgis, and H-P. Herzig, "Near-field imaging of Bloch surface waves on silicon nitride one-dimensional photonic crystals," Opt. Express **16**(8), 5453–5464 (2008).
26. C. Ndiaye, M. Zerrad, A. L. Lereu, R. Roche, P. Dumas, F. Lemarchand, and C. Amra, "Giant optical field enhancement in multi-dielectric stacks by photon scanning tunneling microscopy," Appl. Phys. Lett. **103**(13), 131102 (2013).
27. A. L. Lereu, M. Zerrad, M. Petit, F. de Fornel, and C. Amra, "Multi-dielectric stacks as a platform for giant optical field," Proc. SPIE **9162**, 916219 (2014).
28. A. Shalabney and I. Abdulhalim, "Electromagnetic fields distribution in multilayer thin film structures and the origin of sensitivity enhancement in surface plasmon resonance sensors," Sens. Actuators, A **159**(1), 24–32 (2010).
29. A. Sinibaldi, N. Danz, E. Descrovic, P. Munzert, U. Schulz, F. Sonntag, L. Dominici, and F. Michelotti, "Direct comparison of the performance of Bloch surface wave and surface plasmon polariton sensors," Sens. Actuators, B **174**, 292–298 (2012).
30. W. YuHang, Z. Zheng, S. XiaoGang, B. YuSheng, and L. JianSheng, "Hybrid plasmon waveguide leveraging Bloch surface polaritons for sub-wavelength confinement," Sci. China: Technol. Sci. **56**(3), 567–572 (2013).
31. Z. Sekkat, S. Hayashi, D. V. Nesterenko, A. Rahmouni, S. Refki, H. Ishitobi, Y. Inouye, and S. Kawata, "Plasmonic coupled modes in metal-dielectric multilayer structures: Fano resonance and giant field enhancement," Opt. Express **24**(18), 20080–20088 (2016).
32. R. H. Ritchie, "Plasma Losses by Fast Electrons in Thin Films," Phys. Rev. **106**(5), 874–881 (1957).
33. A. Passian, A. Wig, A. L. Lereu, P. G. Evans, F. Meriaudeau, T. Thundat, and T. L. Ferrell, "Probing large area surface plasmon interference in thin metal films using photon scanning tunneling microscopy," Ultramicroscopy **100**(3-4), 429–436 (2004).

Optics EXPRESS

34. A. Passian, A. L. Lereu, A. Wig, F. Meriaudeau, T. Thundat, and T. L. Ferrell, "Imaging standing surface plasmons by photon tunneling," Phys. Rev. B **71**(16), 165418 (2005).
35. E. Ozbay, "Plasmonics: Merging Photonics and Electronics at Nanoscale Dimensions," Science **311**(5758), 189–193 (2006).
36. A. Archambault, T. V. Teperik, F. Marquier, and J. J. Greffet, "Surface plasmon Fourier optics," Phys. Rev. B **79**(19), 195414 (2009).
37. E. Kretschmann, "The determination of the optical constants of metals by excitation of surface plasmons," Z. Phys. A: Hadrons Nucl. **241**(4), 313–324 (1971).
38. W. A. Challener, J. D. Edwards, R. W. McGowan, J. Skorjanec, and Z. Yang, "A multilayer grating-based evanescent wave sensing technique," Sens. Actuators, B **71**(1-2), 42–46 (2000).
39. K. Toma, E. Descrovi, M. Toma, M. Ballarini, P. Mandracci, F. Giorgis, A. Mateescu, U. Jonas, W. Knoll, and J. Dostalek, "Bloch surface wave-enhanced fluorescence biosensor," Biosens. Bioelectron. **43**, 108–114 (2013).
40. F. Frascella, S. Ricciardi, P. Rivolo, V. Moi, F. Giorgis, E. Descrovi, F. Michelotti, P. Munzert, N. Danz, L. Napione, M. Alvaro, and F. Bussolino, "A Fluorescent One-Dimensional Photonic Crystal for Label-Free Biosensing Based on Bloch Surface Waves," Sensors **13**(2), 2011–2022 (2013).
41. A. Sinibaldi, R. Rizzo, G. Figliozzzi, E. Descrovic, N. Danz, P. Munzert, A. Anopchenko, and F. Michelotti, "A full ellipsometric approach to optical sensing with Bloch surface waves on photonic crystals," Opt. Express **21**(20), 23331 (2013).
42. A. L. Lereu, M. Zerrad, A. Passian, and C. Amra, "Surface plasmons and Bloch surface waves: towards optimized ultra-sensitive optical sensors," Appl. Phys. Lett. **111**(1), 011107 (2017).
43. F. Michelotti, R. Rizzo, A. Sinibaldi, P. Munzert, C. Wachter, and N. Danz, "Design rules for combined label-free and fluorescence Bloch surface wave biosensors," Opt. Lett. **42**(14), 2798 (2017).
44. A. Occhicone, A. Sinibaldi, F. Sonntag, P. Munzert, N. Danz, and F. Michelotti, "A novel technique based on Bloch surface waves sustained by one-dimensional photonic crystals to probe mass transport in a microfluidic channel," Sens. Actuators, B **247**, 532–539 (2017).
45. P. Munzert, N. Danz, A. Sinibaldi, and F. Michelotti, "Multilayer coatings for Bloch surface wave optical biosensors," Surf. Coat. Technol. **314**, 79–84 (2017).
46. A. Sinibaldia, C. Sampaoli, N. Danz, P. Munzert, L. Sibilio, F. Sonntag, A. Occhicone, E. Falvo, E. Tremante, P. Giacomini, and F. Michelotti, "Detection of soluble ERBB2 in breast cancer cell lysates using a combined label-free fluorescence platform based on Bloch surface waves," Biosens. Bioelectron. **92**, 125–130 (2017).
47. Y. Liu, J. Chen, M. Du, X. Wang, X. Ji, and Z. He, "The preparation of dual-functional hybrid nanoflower and its application in the ultrasensitive detection of disease-related biomarker," Biosens. Bioelectron. **92**, 68–73 (2017).
48. M. Ballarini, F. Frascella, F. Michelotti, G. Digregorio, P. Rivolo, V. Paeder, V. Musi, F. Giorgis, and E. Descrovi, "Bloch surface waves-controlled emission of organic dyes grafted on a one dimensional photonic crystal," Appl. Phys. Lett. **99**(4), 043302 (2011).
49. M. Ballarini, F. Frascella, E. Enrico, P. Mandracci, N. De Leo, F. Michelotti, F. Giorgis, and E. Descrovi, "Bloch surface waves-controlled fluorescence emission: Coupling into nanometer-sized polymeric waveguides," Appl. Phys. Lett. **100**(6), 063305 (2012).
50. S. Pirotta, X. G. Xu, A. Delfan, S. Mysore, S. Maiti, G. Dacarro, M. Patrini, M. Galli, G. Guizzetti, D. Bajoni, J. E. Sipe, G. C. Walker, and M. Liscidini, "Surface-Enhanced Raman Scattering in Purely Dielectric Structures via Bloch Surface Waves," J. Phys. Chem. C **117**(13), 6821–6825 (2013).
51. R. Badugu, K. Nowaczyk, E. Descrovi, and J. R. Lakowicz, "Radiative decay engineering 6: Fluorescence on one-dimensional photonic crystals," Anal. Biochem. **442**(1), 83–96 (2013).
52. E. Descrovi, D. Morrone, A. Angelini, F. Frascella, S. Ricciardi, P. Rivolo, N. De Leo, L. Boarino, P. Munzert, F. Michelotti, and F. Giorgis, "Fluorescence imaging assisted by surface modes on dielectric multilayers," Eur. Phys. J. D **68**(3), 53 (2014).
53. K. Ray, R. Badugu, and J. R. Lakowicz, "Bloch surface wave-coupled emission from quantum dots by ensemble and single molecule spectroscopy," RSC Adv. **5**(67), 54403–54411 (2015).
54. R. Wang, Y. Wang, D. Zhang, G. Si, L. Zhu, L. Du, S. Kou, R. Badugu, M. Rosenfeld, J. Lin, P. Wang, H. Ming, X. Yuan, and J. R. Lakowicz, "Diffraction-Free Bloch Surface Waves," ACS Nano **11**(6), 5383–5390 (2017).
55. C. Amra, M. Zerrad, F. Lemarchand, A. L. Lereu, A. Passian, A. Zapien, and M. Lequime, "Energy density engineering via zero admittance domains in all-dielectric stratified materials," Phys. Rev. A **97**(2), 023819 (2018).
56. A. Siabi-Garjan and R. Hassanzadeh, "A computational approach for engineering optical properties of multilayer thin films: Particle swarm optimization applied to Bruggeman homogenization formalism," Eur. Phys. J. Plus **133**(10), 419 (2018).
57. M. Zerrad, A. L. Lereu, C. N'diaye, F. Lemarchand, and C. Amra, "Bandwidths limitations of giant optical field enhancements," Opt. Express **25**(13), 14883 (2017).
58. B. Badoil, F. Lemarchand, M. Cathelinaud, and M. Lequime, "Manufacturing of an absorbing filter controlled with a broadband optical monitoring," Opt. Express **16**(16), 12008–12017 (2008).
59. M. Candille, "Détermination du Critre D'arrêt Pour le Maximtre Monochromatique, Systme de Contrôle Optique de Couches Minces Multidilectriques," Opt. Acta **26**(12), 1477–1486 (1979).
60. B. Badoil, F. Lemarchand, M. Cathelinaud, and M. Lequime, "An Error Compensation Strategy for Broadband Optical Monitoring," in Optical Interference Coatings (Optical Society of America, 2007), p. WC5.

Optics EXPRESS

61. B. Badoil, F. Lemarchand, M. Cathelinaud, and M. Lequime, "Interest of broadband optical monitoring for thin-film filter manufacturing," Appl. Opt. **46**(20), 4294–4303 (2007).
62. H. A. Macleod, Thin-Film Optical Filters, 3rd ed. (Institute of Physics, 2001).
63. B. T. Sullivan and J. A. Dobrowolski, "Deposition error compensation for optical multilayer coatings. I. Theoretical description," Appl. Opt. **31**(19), 3821 (1992).
64. B. T. Sullivan and J. A. Dobrowolski, "Deposition error compensation for optical multilayer coatings. II. Experimental results-sputtering system," Appl. Opt. **32**(13), 2351 (1993).
65. A. Zöller, M. Boos, R. Goetzelmann, H. Hagedorn, and W. Klug, "Substantial progress in optical monitoring by intermittent measurement technique," Proc. SPIE **5963**, 59630D (2005).